Neuron, Volume *72*

Supplemental Information

Glial-Derived Prodegenerative Signaling

in the *Drosophila* Neuromuscular System

Lani C. Keller, Ling Cheng, Cody J. Locke, Martin Müller, Richard D. Fetter, and Graeme W. Davis

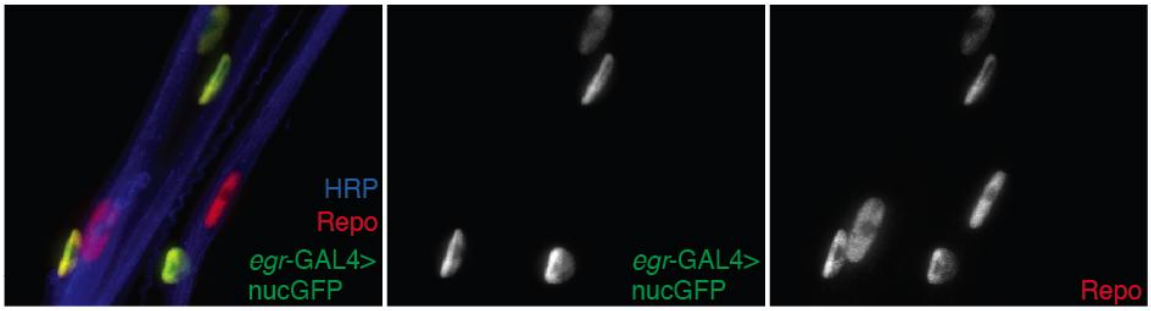

Figure S1. *Eiger*-GAL4 expresses in a subset of peripheral glia.
Representative images of motoneurons expressing nuclear-GFP (green) driven in a subset of peripheral glia by *egr*-GAL4 and stained with Repo (red) to visualize all glia nuclei and HRP (blue) to visualize neuronal membranes.

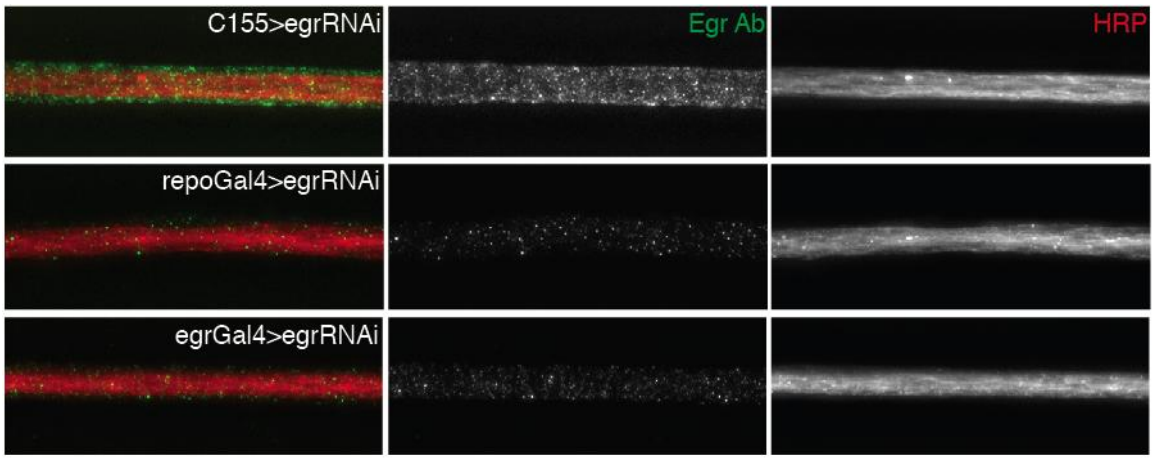

Figure S2. Eiger protein can be knocked down by expression of *Eiger*-RNAi in glia.

Representative images of larval nerve bundles from animals where Eiger levels were knocked down in all neurons using *elav*^{C155}-GAL4 (top panels), all glia using *repo*-GAL4 (middle panels), or a subset of peripheral glia using *egr*-GAL4 (bottom panels).

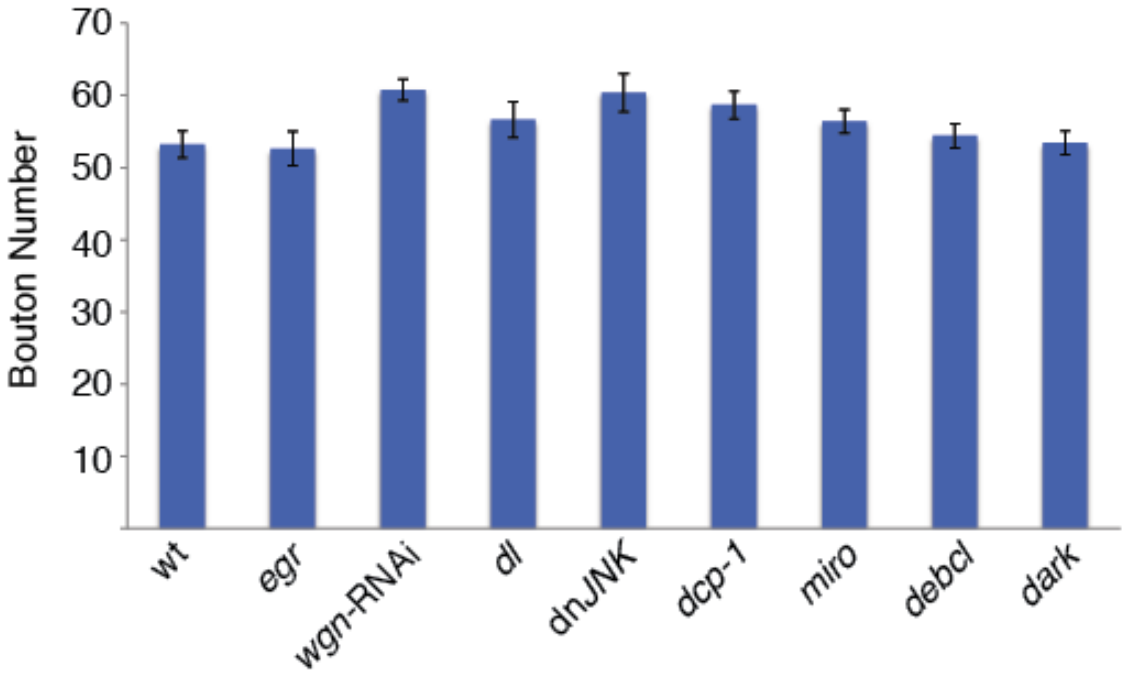

Figure S3. NMJ morphology and growth is not significantly different in any of the mutants used in this study.

Bouton numbers were counted in third instar larval muscle 6/7 at segments A2 and A3. Wt = w^{1118} (n = 34 muscles); *egr* = $eiger^{\Delta 25}/eiger^{\Delta 25}$ (n = 29 muscles); *wgn*RNAi = $elav^{C155}$-GAL4/+; *wgn*RNAi/+ (n = 24 muscles); *dl* = dl^{1}/dl^{1} (n = 40 muscles); *dn*JNK = $elav^{C155}$-GAL4;*dnbsk* (n = 24 muscles); *dcp-1* = $dcp1^{Prev1}/dcp1^{Prev1}$ (n = 24 muscles); *miro* = $miro^{B682}/miro^{B682}$ (n = 36 muscles); *debcl* = $debcl^{[E26]}/debcl^{[E26]}$ (n = 20 muscles); *dark* = $dark^{CD4}/dark^{CD4}$ (n = 20 muscles). Error bars represent SEM.

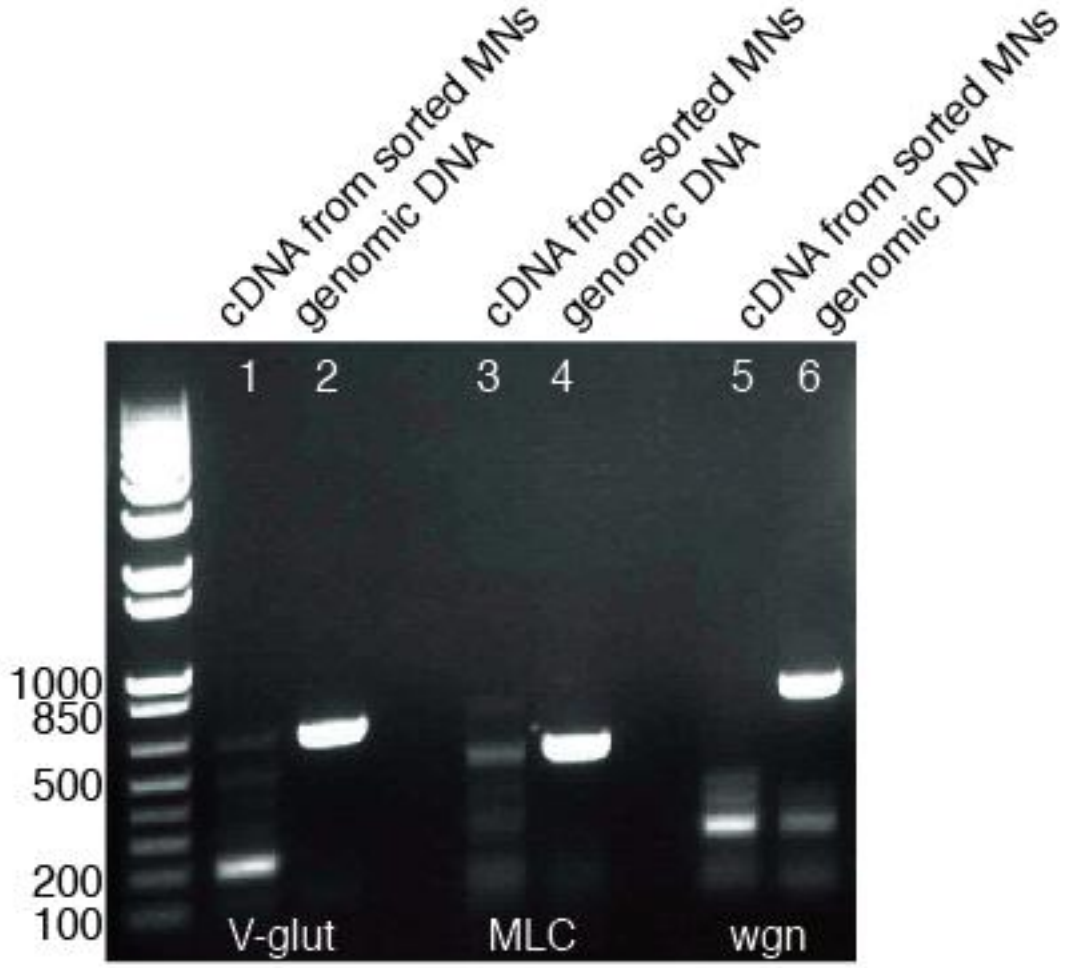

Figure S4. *wengen* cDNA is expressed in motoneurons.

cDNA was synthesized from RNA isolated from a FACS sorted motoneuron population of third instar larval brain. V-glut, a known motoneuron-specific protein, was used as a positive control (lane 1, V-glut cDNA = 208bp; lane 2, V-glut from genomic DNA = 652bp) and myosin light chain 2, a muscle-specific gene, was used as a negative control (lane 3, no MLC cDNA expressed since expected band = 365bp; lane 4, MLC from genomic DNA = 524bp). Wengen is expressed in motoneurons (lane 5, wengen cDNA = 224bp; lane 6, wengen from genomic DNA = 797bp).

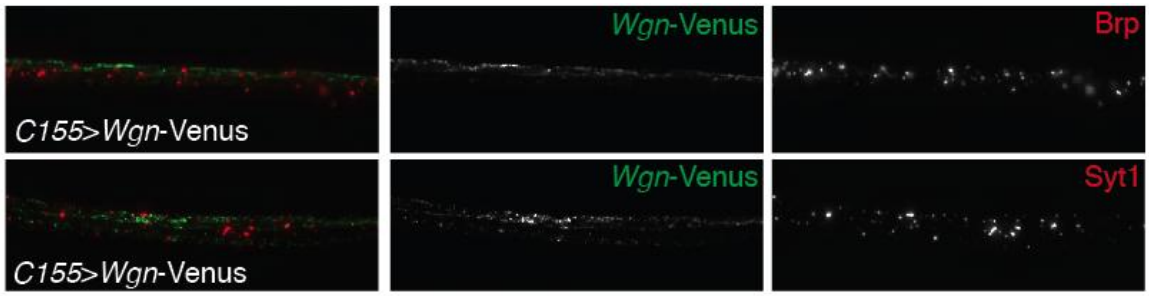

Figure S5. Wengen-Venus expressed in neurons does not co-localize with Brp or Syt1.

Representative images of nerve bundles from animals expressing *Wgn*-Venus in all neurons (green) and stained with either Brp (red, top panel) or Syt 1 (red, bottom panel).

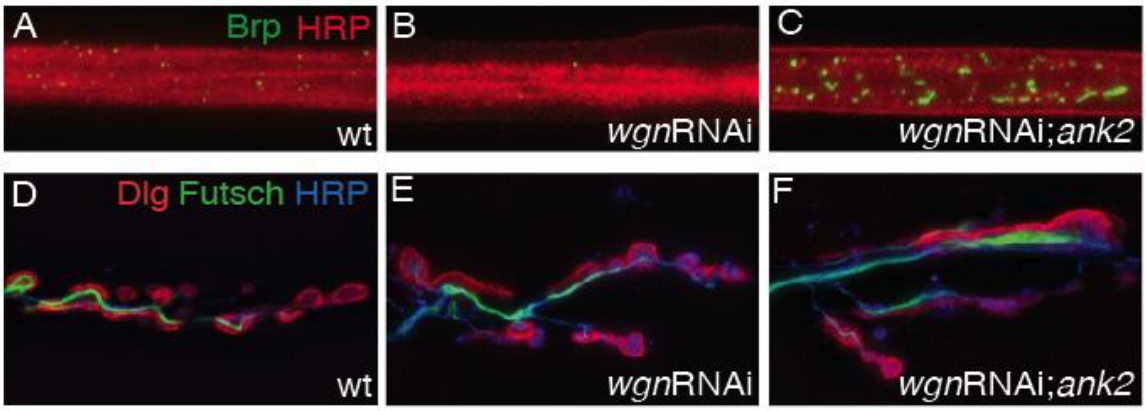

Figure S6. Knockdown of presynaptic *wengen* suppresses *ank2* dependent degeneration despite persistent cellular stresses.

(A-C) Representative images of individual third instar nerve bundles stained for the neuronal membrane marker HRP (red) and the active zone marker Brp (green), which accumulates in *ank2* mutant axons. All images were taken at the same time with the same exposure conditions. (A) Wild-type nerve bundle with no visible Brp accumulations. (B) Nerve bundle from an animal with *wgn*RNAi expressed presynaptically that looks similar to wild-type with no visible Brp accumulations. (C) Nerve bundle from an *ank2* mutant animal with neuronal knockdown of *wgn*, showing significant axonal Brp accumulations, similar to the *ank2* mutant alone. Total Brp fluorescence intensity integrated over total nerve area are the following: Wt = w^{1118} (n = 17 nerve bundles; average 8.16 arbitrary units); *wgn*RNAi = $elav^{C155}$-GAL4/+; *wgn*RNAi/+ (n = 11 nerve bundles; average 5.0 arbitrary units); *wgn*RNAi;*ank2* = $elav^{C155}$-GAL4/+; *wgn*RNAi/+; *ank2/ank2* (n = 11 nerve bundles; average 28 arbitrary units). *ank2* and *wgn*RNAi*;ank2* both have significantly more Brp total fluorescence than either wild-type or *wgn*RNAi alone ($p<0.001$). P values were determined using one-way ANOVA with post-hoc

Tukey-Kramer. Statistical differences remain when comparisons are made using Student's t test. (D-F) Representative images of third instar muscle 6/7 NMJs stained for the neuronal microtubule-associated protein Futsch (green), the presynaptic membrane marker HRP (blue), and the postsynaptic marker Dlg (red). (D) A wild-type NMJ shows an elongated and organized Futsch-positive microtubule cytoskeleton. (E) An NMJ expressing *wgn*RNAi presynaptically also shows an elongated and organized Futsch-positive microtubule cytoskeleton. (F) An NMJ mutant for *ank2* and expressing neuronal *wgn*RNAi shows disorganized Futsch staining with accumulations within boutons.

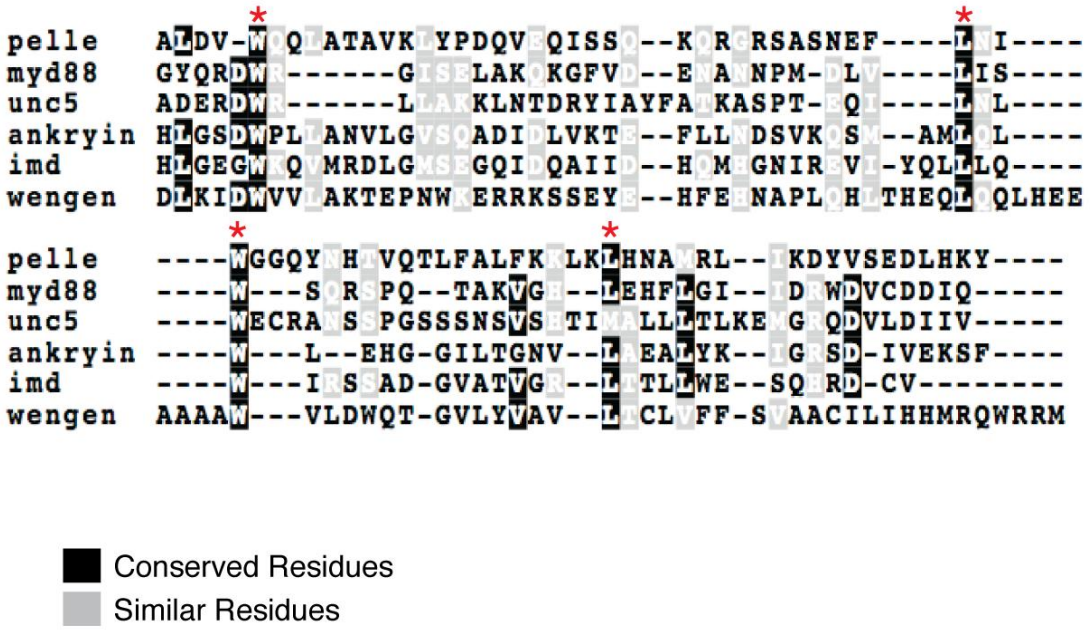

Figure S7. Alignment of *Drosophila* death domain proteins demonstrating significant homology with Wengen, the TNFα receptor.

Amino acid sequence comparison of Wengen with other Death Domain containing proteins in the *Drosophila* genome. Conserved residues are highlighted in black and similar residues are indicated in gray. Red asterisks mark critical residues shown previously to be necessary for apoptotic signaling (McDonald et al., 2001). The following *Drosophila* proteins were used: Pelle (CG5974), Myd88 (CG2078), Unc5 (CG8166), Ankyrin (CG1651), Imd (CG5576), and Wengen (CG6531). Protein alignment was conducted using ClustalW2-Multiple Sequence Alignment program.

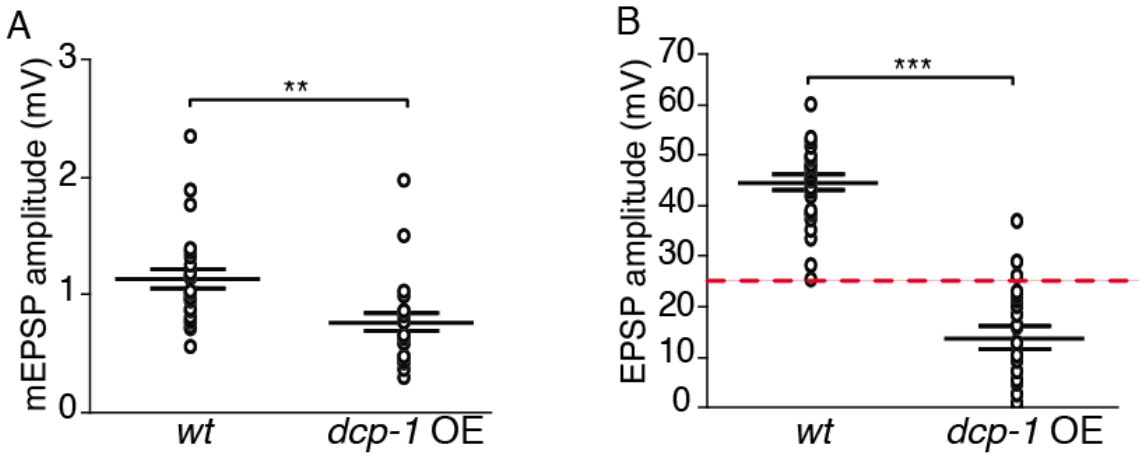

Figure S8. Expression of Dcp-1 in neurons causes significant synaptic transmission deficiencies.

(A) Average mEPSP amplitude for wild-type and Dcp-1 expressed pan-neuronally with *C155*-GAL4. Values representing averages from individual recordings are shown as open circles and genotypic averages are shown by large horizontal bar. Wt = w1118 (average mEPSP = 1.23mV, n=26); *dcp-1 OE* = *elav*^{C155};*pUAS-Dcp-1/+* (average mEPSP = 0.79, n = 23). (B) Average EPSP amplitude for wild-type and Dcp-1 expressed pan-neuronally with *C155*-GAL4. There are a large number of recordings below 25mV, the wild-type limit (indicated by dashed red line). Wt = w1118 (average EPSP = 44.2mV, n=26); *dcp-1 OE* = *elav*^{C155};*pUAS-Dcp-1/+* (average EPSP = 13.4, n = 23). Error bars represent SEM; P values were determined using Student's t test: **, P<0.01; ***, P<0.001.

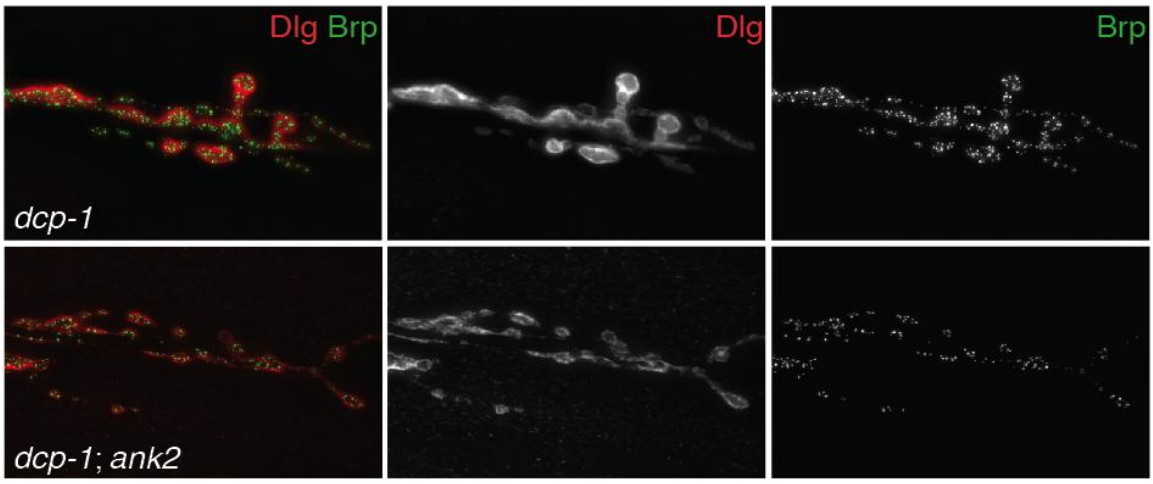

Figure S9. A null mutation in *dcp-1* suppresses *ank2* dependent neuronal degeneration at the *Drosophila* NMJ.

Representative images of third instar muscle 6/7 NMJs stained with the presynaptic active zone marker Brp (green) and the postsynaptic marker Dlg (red). *dcp-1* null mutations do not affect NMJ morphology or co-localization of Brp (green) and Dlg (red) at muscle 6/7 (top panels). Animals that are homozygous for both *dcp-1* and *ank2* have a remarkably improved NMJ in comparison to *ank2* animals alone (bottom panels).

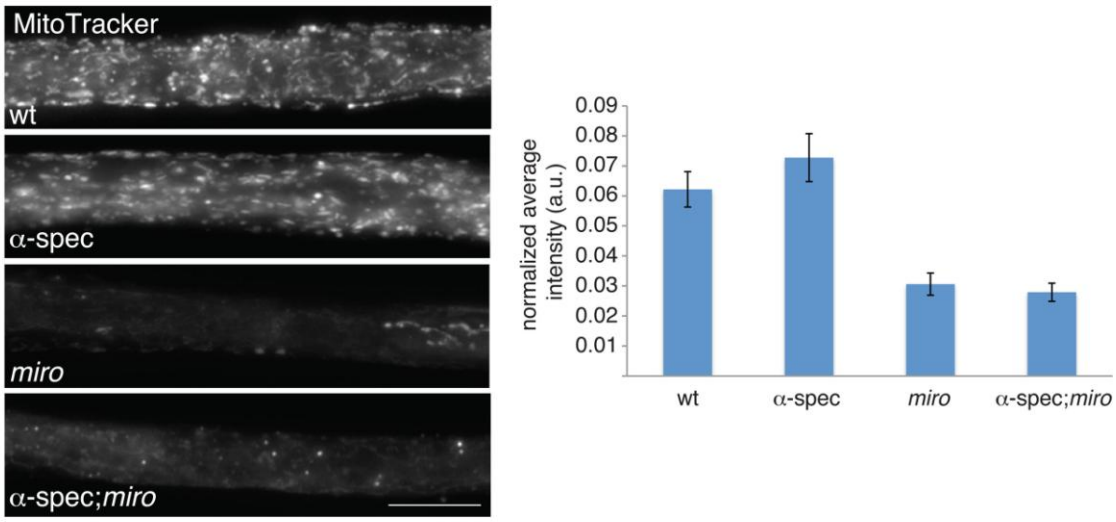

Figure S10. Mitochondria are depleted from peripheral nerves in *miro* mutant animals. A representative image of a peripheral nerve is shown for each indicated genotype. Nerves are stained with MitoTracker to reveal mitochondrial content. The images are a projection of a 3D confocal image stack. Scale bar = 10µm. Sample sizes are as follows: wild type N=11; *miro* N=13; *α-spectrin* RNAi driven in motoneurons (*α-spec*) N=10; *α-spectrin* RNAi expressed in the *miro* mutant background (*α-spec*; *miro*) N=10. The graph shows quantification of the change in MitoTracker fluorescence in the different genotypes. The *miro* mutation shows significantly diminished axonal MitoTracker staining compared to wild type and *α-spec* RNAi animals. There is no significant difference comparing *miro* with *α-spectrin* RNAi expressed in the *miro* mutant background. Methods for labeling peripheral motoneurons with Mitotracker Red are as follows. MitoTracker Red CMXRos (Invitrogen, M7512; 100nM) was added to dissected third instar larvae. Axons were cut distally to allow entry of MitoTracker into the motor axons. Preparations were incubated for 30 minutes at room temperature, washed in HL3 for 1hr and imaged. All genotypes were dissected and imaged at the same time with identical image acquisition parameters.

Supplemental Experimental Procedures

Fluorescence Recovery After Photobleaching (FRAP)

FRAP experiments were performed within single axons projecting to muscle 4 (segments A2 and A3) of wandering third instar larvae. A small axon region (3x1.5μm, spanning the diameter of the axon) was bleached using a confocal laser-scanning system (Ultima, Prairie Technologies). Excitation light (488 nm) was focused onto the specimen using a 100 × objective (1.0 NA, Olympus), and emitted light was detected with a gallium arsenide phosphide-based photocathode photomultiplier tube (Hamamatsu). Images were sampled at 4Hz, and acquisition frequency was decreased to 0.5 Hz for the last 20 images. Eight data points were acquired before photobleaching. The time required for bleaching was <0.3 sec and was negligible compared to the duration of recovery. For FRAP analysis, background-corrected average fluorescence levels in the bleached area of the axon ("F") were normalized to the background-corrected average fluorescence measured in two unbleached axonal regions ("F_0") using custom-written routines in Igor Pro (Version 6.22A, WaveMetrics, Inc.). Only axons displaying >70% photobleaching relative to initial fluorescence in the bleached area and a global photobleaching during image acquisition <15% were used for analysis. All data were corrected for photobleaching during image acquisition. Fluorescence recovery was fit with single and double exponential functions. The fit was considered biexponential if both the ratio of the two time constants was more than two and if the amplitude of each exponential component contributed at least 15% to the total amplitude.